ELSEVIER

Polymer 43 (2002) 4185–4196

polymer

www.elsevier.com/locate/polymer

The thermomechanical environment and the microstructure of an injection moulded polypropylene copolymer

J.C. Viana[a,*], A.M. Cunha[a], N. Billon[b]

[a]*Department of Polymer Engineering, University of Minho, 4800-058 Guimarães, Portugal*
[b]*Centre de Mise en Forme des Matériaux, UMR CNRS 7635, École des Mines de Paris, BP207 06904, Sophia-Antipolis, France*

Received 23 January 2002; accepted 3 April 2002

Abstract

The microstructure of an injection moulding propylene copolymer is varied through systematic changes on the processing conditions (melt and mould temperatures and injection flow rate). The skin-core structure was characterised by several experimental techniques. The skin ratio was assessed by polarised light microscopy. The morphological features of the skin layer (level of crystalline phase orientation, degree of crystallinity, β-phase content and double texture) were evaluated by wide-angle X-ray diffraction. The core features (degree of crystallinity and lamella thickness) were assessed by differential scanning calorimetry. The thermomechanical environment imposed during processing was characterised by mould filling simulations. The thermal and shear stress levels were evaluated by a cooling index and the wall shear stress. The results show the relationship between these and the microstructural features. The microstructure development is then interpreted considering the constrictions imposed during processing, being assessed by thermomechanical indices. Furthermore, the direct connections between these indices and the degree of crystallinity of the core and the level of orientation of the skin are verified.

Keywords: Injection moulding; Thermomechanical environment; Microstructure

1. Introduction

In the injection moulding process, a hot polymer melt is forced under pressure to flow between cold mould walls. The high viscous melt has a complex behaviour (e.g. shear thinning and viscoelastic nature) and a low thermal diffusivity. As a consequence, the process is characterised by an unsteady and non-isothermal flow, a high and local viscous dissipation and a spatial variation of the viscosity. Furthermore, the molten polymer can also experience the effect of significant normal stresses, especially at the flow front and in zones of pronounced geometry variation. As a result of these effects the obtained moulding has a microstructure gradient through the thickness, varying also along the respective flow path. This microstructure determines, to some extent, the mechanical behaviour of the mouldings.

The microstructure developed by semicrystalline thermoplastics when cooled down under specific thermomechanical conditions, namely shear fields and important thermal gradients, is widely reported in the literature [1–14]. This structure features a hierarchy of macromolecular arrangements and a through-the-thickness morphological gradient, which in a simple description is composed of:

(i) two external highly oriented skin layers (in the case of polyolefins constituted by a peculiar shish–kebab crystalline structure [14–16]);
(ii) a central spherulitic core.

Between these two layers a transition zone is commonly found presenting deformed spherulite structures typically associated to the crystallisation under high shear and temperature gradients. The local thermomechanical environment imposed during processing dictates the relative dimensions and the morphology of these layers.

This work explores the development of the microstructure of an injection moulding propylene copolymer under the local thermomechanical environment imposed during processing, in terms of microstructural features associated to the skin and core layers.

* Corresponding author. Tel.: +351-252-510-249; fax: +351-253-510-249.
E-mail address: jcv@dep.uminho.pt (J.C. Viana).

0032-3861/02/$ - see front matter
PII: S0032-3861(02)00253-7

2. Microstructure of injection moulded semicrystalline polymers

2.1. Skin layers

The skin layers start forming during the filling phase due to the rapid cooling of the hot and very oriented melt against to the cold mould walls (development of the frozen layer). When observed by polarised light microscopy (PLM), the skin has a homogeneous appearance with no discernible morphological features. However, it has a peculiar microstructure, characteristic of a crystallisation under high stress fields and cooling rates, normally referred to as shish–kebab structures [14–16]. The shishes are bundles of macromolecules in rows oriented in the flow direction. The kebabs grow perpendicular to the shish axis, as intercalated disks. These are constituted of chain-folded macromolecules, as in a lamellar structure. For polypropylene, subsidiary kebabs grow near perpendicularly on the main ones (similarly to the epitaxial growth in spherulite-like crystallisation). Therefore, in a shish–kebab structure, the macromolecules are oriented parallel (shish and main kebabs) and perpendicular (subsidiary kebabs) to the flow direction, showing a mixed crystallographic *c*- and a^*-axis orientation components. The amorphous phase, normally highly strained, fills in the space between the crystalline one [15]. The crystalline lamellar matrix is linked by tie molecules. The skin material crystallises essentially in the α-form, although a small amount of β-form can also be found [14].

The skin thickness is controlled by the combined effect of the cooling rate and of the stress fields imposed to the melt. Its formation is thermally controlled for higher melt temperatures and governed by the shear stress level for the lowest melt temperatures [17,18]. Thicker skins are promoted by lower moulding temperatures (melt and mould) and flow rates and by higher pressures [3,10,11,17,18].

The skin layer shows a fibre like orientation with the molecular chain axis (*c*-axis) preferentially oriented in the flow direction (FD). The maximum of the molecular orientation is not found generally at the surface of the sample, but somewhere in the interior of the skin, depending on the shear fields associated to the specific moulding conditions [5,7,12]. The final molecular orientation of the skin is favoured by the decreasing in the melt and mould temperatures [7,11]. For polypropylene, it was found to be higher for the combination of low melt and high mould temperatures, but also with the decrement of the flow rate together with a low melt and mould temperatures and low holding pressure [19]. The effect of the injection flow rate on the level of orientation is rather contradictory, as a result of the viscous dissipation behaviours of different material grades [11,20]. The level of orientation was also reported to increase with the holding pressure [21]. The a^*-axis orientation increases with the melt temperature, independent of the molecular mass of PP [10]. Furthermore, the fraction of this a^*-axis oriented component also increases with the melt temperature, the lowering of the molecular mass and by copolymerisation with ethylene [10]. These known dependences reveal the importance of the relaxation process of the material between the end of filling and the crystallization onset for the development of the molecular orientation.

2.2. Core layer

The core zone shows essentially an α-type spherulitic morphology, typical of melts that crystallise in almost quiescent conditions. The previously crystallised material acts as an insulation barrier due to its low thermal conductivity, leading to a slower cooling rate in the core, which is minimum at the core centre. Consequently, the core has generally a high crystallinity, showing a spherulite size gradient (typically of the order of 1–10 μm of diameter) with dimensions increasing towards the central zone. In its exterior zone the spherulites can be elongated (oblate spherulites) with the higher axis perpendicular to the flow direction due to the imposed cooling gradient [3,22]. The slower crystallisation process in the core is mainly thermally controlled. The final degree of crystallisation of the core decreases with increasing cooling rate and for low melt temperatures [10,23]. In general, the skin has a lower crystallinity than the core [10,23]. Sometimes a rather flat crystallinity profile through the thickness of the mouldings can be obtained, which is not affected by the injection speed, the mould temperature and the holding time [11]. Due to the slower cooling rates, the core has almost no preferred molecular orientation.

The spherulite size of the core is mainly controlled by the nucleation process [24], decreasing for faster cooling rates, which lowers the crystallisation temperature and promotes nucleation. The total number of potential nuclei can be extremely reduced by increasing the superheating level (higher temperature or time at a given temperature superior to the thermodynamic melting temperature), leading to spherulites of higher diameter. The spherulite size has been observed to increase with the melt and mould temperatures owing to the slower nucleation rates [8,11]. It was found to increase with injection speed, due to the increase in the temperature by viscous dissipation [11]. But a decrease in the spherulite size with the injection velocity was also reported, as a result of the higher nucleation caused by the orientation induced by the flow [8]. A non-consistent variation of the spherulite dimensions with the holding time was also observed, depending on material properties (e.g. the molecular weight) [11].

The imposed thermomechanical environment during processing also influences the thickness of the core lamellae. They increase with decreasing of the undercooling degree, or increasing of crystallisation temperature. They are also thicker as the pressure is higher [25]. A slight variation of the lamella thickness with the mould temperature was observed [16].

2.3. Transition zone

The evolution from the skin to core is progressive, and sometimes a transition zone can be defined in between (also called shear zone). The morphology and thickness of this zone are mainly dependent on the holding stage conditions of the moulding cycle. In this zone, the spherulites can be deformed in the flow direction due to the effect of shear. A high density of β-type spherulites is generally found in this zone. This crystalline form is favoured by shear and low temperatures [8,12]. An increased concentration of the β-spherulites was reported for high injection rates [11]. Its amount was also observed to be higher for low melt temperatures in the absence of a high molecular alignment [10,14].

The degree of crystallinity in the transition zone is noticeably affected by the holding pressure. An increase on it acts as a quenching phenomenon (the pressure increases the thermodynamic melting temperature originating a higher undercooling degree), which can locally reduce the degree of crystallinity [5]. However, a maximum of crystallinity on the transition zone was observed, which shift towards the sample middle-plane with decreasing flow rate [26]. This was explained by the combined effect of the flow-induced crystallisation and of the pressure on the crystallisation temperature.

The molecular orientation profile in the thickness direction can present shoulders or local maxima in the shear zone. These are formed during the holding stage, due to the low velocity flow under relatively low temperatures and the reduction on the molecular mobility by pressure [5,7].

3. Thermomechanical environment in injection moulding

In injection moulding, the thermomechanical environment imposed to the polymer is associated with the combined effect of a particular set of processing variables (machine setting), mould geometry (feeding system, flow type and part geometry) and thermorheological properties of the material. As a result, specific fields of pressure, temperatures, shear rates and stresses are developed. These can be estimated by computer simulations of the injection moulding process or by adequate mould instrumentation (local pressures and average temperatures). From the simulations the local through-the-thickness profiles of the temperature and of the shear stress at the end of the filling stage can be computed. Fig. 1 shows typical profiles of these variables (in the simulations the effect of heat released by crystallisation was not included), which can be associated, respectively, to the thermal and shear stress levels applied during processing.

Using a straightforward and simplified approach, the global temperature profile can be, respectively, single

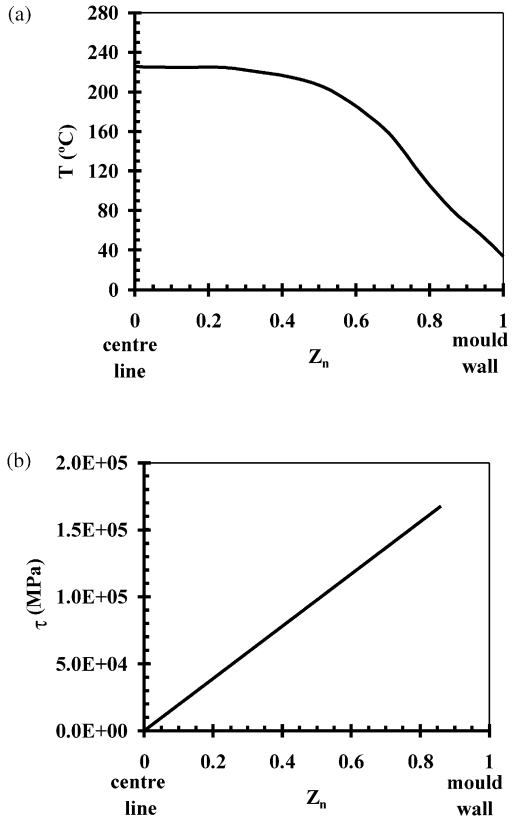

Fig. 1. Typical profiles of the temperature (upper), T, and the shear stress (lower), τ, computed at the end of the filling phase (axi-symmetric dumbbell-like specimen of 1.5 mm of diameter moulded in a propylene copolymer; Z_n is the normalised thickness).

numbered by the global bulk temperature, T_{bg} (velocity weighted average temperature, which takes into account convective effects [18,27]):

$$T_{bg} = \bar{T}_{bg} + \frac{\int_0^h (T - \bar{T}_{bg}) v(z) \mathrm{d}z}{\frac{1}{h}\int_0^h v(z) \mathrm{d}z} \quad (1)$$

where $\bar{T}_{bg}$ is the average bulk temperature, $v(z)$ the local velocity, h the half-thickness of the moulding, and z is the through-the-thickness direction. T_{bg} is mainly sensitive to the higher central temperatures. The shear stress profile varies almost linearly through the moulding thickness. It can be quantified by the maximum shear stress at the solid/melt interface, τ_w.

4. Experimental

4.1. Material and moulding programme

Axi-symmetrical dumbbell-like specimens of 1.5 mm of diameter were injection moulded using a propylene-ethylene sequential copolymer (APPRYL 3120 MR5). This commercial polymer has a narrow molecular weight

distribution, and incorporates about 8% of ethylene, being typically used in automotive applications.

The moulding programme was defined accordingly to a central composite experimental design, including variations in three levels of the melt temperature ($T_{inj} = 200$, 230, 270 °C), the mould temperature ($T_w = 5$, 30, 80 °C) and the flow rate ($Q_{inj} = 2$, 4, 10 cm^3/s). Details can be found elsewhere [18,28]. The mouldings were identified by a reference code, corresponding to the processing variables used, in the following order: $T_{inj}/T_w/Q_{inj}$.

4.2. Sample preparation

Three different samples were prepared from the central zone of the cylindrical region of each moulded axisymmetric specimen: a thin microtomed cross-section of the overall specimen, and a separated skin and core samples. The cylindrical zone of the specimens was immersed in a cold cure epoxy resin (COLDFIX®), which was allowed to cure for 72 h at room temperature. This was intent to give more support to the subsequent cutting procedures.

Cross-sections of approximately 15 μm thick were cut transversely to the flow direction from the centre of the immersed specimens, using a microtome equipped with steel razor blades. The microtomed sections (of the specimen only, since it was automatically separated from the epoxy resin during the microtome operation) were placed between glass slides using a fluid of matching refractive index (Canada Balsam).

Cylindrical samples of the core only were obtained by carefully removing the outer skin (defined as the external non-spherulitic zone) of the specimens by manually polishing with grinding paper of sequentially lower grain sizes.

The immersed specimens were also carefully polished along their major length (that is in the FD) in a polishing machine with grinding paper of sequentially lower grain sizes. The thickness of the remainder sample was repeatedly measured, in order to obtain a final thickness equivalent to the measured skin layers. A thin film sample of the skin parallel to FD was obtained.

4.3. Microstructure characterization

The microtomed samples were observed under the polarised light microscope (PLM). The skin thickness was measured in 10 different points along the sample perimeter, with a maximum experimental scattering of 8.0% (average error of 6.6%). An average value was calculated. The skin ratio, Sa, was defined as the quotient between the cross-sectional area of the skin to the total of the sample.

The microtomed sections were also used to estimate the spherulite size, using a small angle light scattering system (H_v set-up), equipped with a HeNe laser (10 mW of power and 632.8 nm of wavelength). The spherulite size is inversely proportional to the dimensions of the four lobes scattered pattern [29]. The average relative dispersion on the measurements was 14.1% (maximum error of 21.0%).

The thermal behaviour of the core samples was studied by differential scanning calorimetry (DSC), in a Perkin–Elmer DSC-7 at the heating rate of 10 °C/min, in a nitrogen atmosphere. From the DSC thermograms were calculated the enthalpy of fusion, ΔH (the area below the DSC thermogram, between the lower and upper limit temperatures of 90 and 175 °C), and the melting (peak) temperatures T_m. The estimated experimental errors were of 5.2 and 0.3%, respectively. The degree of crystallinity of the core, χ_c, was calculated from the ratio $\Delta H/\Delta H_c$. ΔH_c was calculated from the theoretical values of the enthalpies of fusion of polypropylene and polyethylene (respectively, $\Delta H_0^{PP} = 148$ J/g [30] and $\Delta H_0^{PE} = 296$ J/g [31]) and the percentage of incorporation of ethylene in the copolymer (8%), assuming a linear law of mixture. A value of $\Delta H_c = 159.84$ J/g was obtained. Although, this procedure can be controversial and the definition of ΔH_c for a copolymer questionable, it was followed to take into account the influence of the small polyethylene peak on the total crystallinity of the samples.

The lamella thickness was estimated by rearranging the Thompson–Gibbs equation, assuming the general case where the lamellas are much larger than thick [32]:

$$l_c = \frac{2\sigma_e}{\Delta H_c \rho_c} \frac{T_f^0}{(T_f^0 - T_m)} \quad (2)$$

where σ_e is the surface energy of the basal surface of the lamella (associated with the energy of chain folding during the crystallisation process) and ρ_c is the density of the crystalline phase. These values were taken from the literature, for the case of PP: $\rho_c = 0.946$ g/cm^3, $\sigma_e = 122$ mJ/m^2, $\Delta H_c = 148$ J/g [30]. T_f^0 is the thermodynamic melting point of a crystalline lamella of infinite thickness, which was experimentally determined to be $T_{f0} = 181.9$ °C, from the classical Hoffman–Weeks plots in the crystallisation temperature range 125–130 °C. Some doubts exists about the accurate determination of the lamella thickness by DSC measurements, for instances due to the uncertainty in obtaining the exact values of σ_e, T_f^0 and ΔH_c [32]. However, this approach has been followed by several authors to estimate the dimensions of the lamella [33,34] and seems to give good estimate for the order of magnitude.

Wide-angle X-ray diffraction (WAXD) experiments were performed in the skin samples. Ni-filtered Cu Kα radiation was used with the incident X-ray beam normal to the surface of the samples sectioned parallel to FD. Two types of set-ups were used, both in transmission mode. Firstly, the complete diffracted patterns were obtained in a flat-film camera (Debye patterns). Then, the same samples were also mounted in a goniometer and θ–2θ scans were carried out in the range 5–40°, in steps of 0.02°. The curves were analysed in terms of the indices defined in Table 1, from the relative peak heights of the selected diffraction planes (after correction for background and amorphous scattering and thickness effects), accordingly to the procedure outlined elsewhere [12,19,35].

Table 1
Definition of the indices used in the analysis of the θ–2θ X-ray intensity scans [12,19,35]

Index	Definition
Orientation indices	$A_{110} = I_{110}/(I_{110} + I_{111} + I_{131+041})$
	$A_{130} = I_{130}/(I_{130} + I_{111} + I_{131+041})$
Double epitiaxility index	$C_\alpha = I_{040}/(I_{110} + I_{140} + I_{130})$
β-Phase concentration index	$\beta_{300} = I_{300}/(I_{110} + I_{040} + I_{130} + I_{300})$

The errors on the peak intensity measurements are estimated at 5%. In Table 1, the A_{110} and A_{130} indices are related to the orientation of α crystallites in the flow direction. For highly oriented samples $A = 1$; a value of $A = 0.57$ was obtained for isotropic samples of isotatic polypropylene [35]. In this work, the orientation level of the skin, Ω_s, was evaluated as the average between these two orientation indices. The C_α index characterises the epitaxial orientation (double texture) of the α-PP crystallites. C_α is equal to the unity for pure a^*-axis orientation of the crystallites, otherwise $C_\alpha < 1$. The β_{300} index describes the concentration of β-spherulites: pure β-PP would yield $\beta_{300} = 1$.

The degree of crystallinity of the skin was also determined from the θ–2θ scans. The areas under each intensity scan curve, S_{tot}, and under the crystalline peaks, S_{crys} (after subtracting the amorphous scattering) were measured. The degree of crystallinity, χ_s, is given by:

$$\chi_s = \frac{S_{crys}}{S_{tot}} \tag{3}$$

5. Thermomechanical environment quantification

The thermomechanical variables were calculated in a commercial mould filling simulation package, C-MOLD, considering only the filling stage. The results at the end of filling were considered. A complete finite element mesh of the moulding was used (cavities plus feeding system). The rheological behaviour of the melt was experimentally assessed by capillar rheometry [28]. In the simulations the material was assumed as a temperature dependent shear thinning fluid, with the viscosity, η, given by:

$$\eta = 2.042 \times 10^4 \dot{\gamma}^{-0.650} e^{(-8.420\times10^{-3}T)} \tag{4}$$

where $\dot{\gamma}$ is the shear rate (s^{-1}), and T is the temperature (°C). The effect of the released heat of crystallisation during solidification was not included in the simulations despite it should locally disturb the temperature profile.

A bulk temperature of the skin and core layers, respectively, T_{bs} and T_{bc}, were calculated according to Eq. (1), by changing adequately the integration limits [36]. The thermal level of core of the mouldings was estimated by the cooling index, Y_c [28,36]:

$$Y_c = \frac{T_{bc} - T_c}{T_{bc} - T_i} \tag{5}$$

where T_c is the crystallisation temperature (assumed constant) and T_i is the mould/polymer interface temperature (average temperature weighed by the different thermal effusivities of the two materials) [36].

The applied shear stress level was estimated by τ_w. This value is also an indirect indication of the orientation induced by flow.

6. Results

In Table 2 are listed the results of the microstructure characterization and of the thermomechanical environment quantification. They are also resumed in Figs. 3, 5 and 10, showing their variations with Y_c and τ_w.

6.1. Thermomechanical environment

Fig. 2 evidences a strong coupling between the thermal and mechanical phenomena in injection moulding. In a general manner, to a low thermal level (that is, low Y_c) corresponds a high shear stress level and vice-versa. This confirms that the degree of crystallinity of the core and the level of orientation of the skin cannot be controlled independently in conventional injection moulding.

6.2. Skin characteristics

6.2.1. Skin ratio

Fig. 3 depicts the evolution of the skin thickness (observed by PLM) with both thermal and mechanical levels. The skin ratio, Sa, increases with decreasing Y_c and the increment on τ_w.

These relationships are summarised in Fig. 4 that shows the variations of Sa with both these variables. Sa is maximised for the lowest Y_c and highest τ_w values, being minimum for the opposite conditions.

The dependence of Sa upon Y_c is stronger for higher

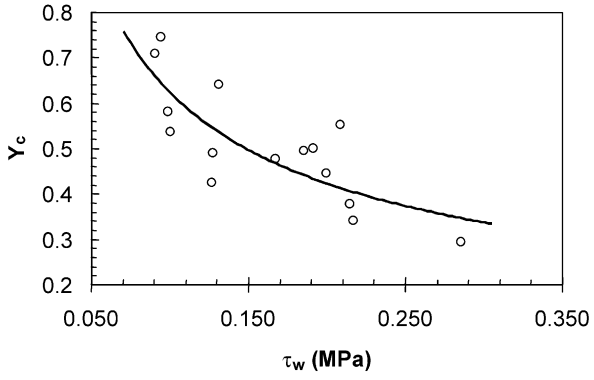

Fig. 2. Relationship between the thermal (Y_c) and the shear stress (τ_w) levels of the mouldings.

Table 2
Thermomechanical environment and microstructure (skin and core) characterizations of the mouldings (Ref.—reference of the moulding condition, Max.—maximum value, Min.—minimum value, Var.—percentage of variation, Y_c—cooling index of the core (thermal level), τ_w—wall shear stress (stress level), Sa—skin ratio, Ω_s—skin orientation index, χ_s—degree of crystallinity of the skin, C_α—double texture index of the skin, β_{300}—β—phase index of the skin, χ_c—degree of crystallinity of the core, l_c—lamella thickness of the core; n.m.—value not measured)

Ref.	Thermomechanical environment		Skin					Core		
$T_{inj}/T_w/Q_{inj}$	Y_c	τ_w (kPa)	Sa	Ω_s	χ_s	C_α	β_{300}	χ_c	l_c (nm)	R_s (μm)
200/5/40	0.342	217	0.343	0.850	0.511	0.457	0.044	0.491	18.3	2.4
200/5/5	0.295	285	0.642	0.865	0.555	0.450	0.025	0.464	17.4	2.2
200/30/10	0.377	215	0.494	0.871	0.503	0.431	0.031	0.507	17.8	2.3
200/80/40	0.551	209	0.313	0.833	0.563	0.418	0.028	0.511	18.3	1.7
200/80/5	0.501	191	0.627	0.812	0.523	0.456	0.017	0.524	17.2	3.2
230/5/10	0.425	127	0.356	0.835	0.379	0.436	0.022	0.487	17.7	2.6
230/30/40	0.494	185	0.233	0.867	0.449	0.419	0.040	0.501	18.1	3.1
230/30/10	0.475	168	0.331	n.m.	n.m.	n.m.	n.m.	0.494	17.8	2.3
230/30/5	0.445	200	0.438	0.853	0.472	0.473	0.026	0.519	17.7	2.9
230/80/10	0.640	131	0.318	0.758	0.474	0.497	0.020	0.518	18.3	2.0
270/5/40	0.536	100	0.175	0.751	0.469	0.447	0.046	0.512	18.1	3.5
270/5/5	0.489	128	0.379	0.705	0.423	0.490	0.043	0.493	18.1	2.0
270/30/10	0.580	99	0.268	0.725	0.434	0.507	0.036	0.494	18.2	2.6
270/80/40	0.746	94	0.114	0.768	0.449	0.518	0.055	0.516	18.6	2.1
270/80/5	0.708	90	0.333	0.681	0.488	0.535	0.028	0.514	18.1	1.9
Max.	0.746	285	0.642	0.871	0.563	0.535	0.055	0.524	18.6	3.5
Min.	0.295	90	0.114	0.681	0.379	0.418	0.017	0.464	17.2	1.7
Var (%)	153	216	463	28	49	28	230	13	8	106

values of Y_c. Conversely they are much less accentuated for the lowest Y_c. The skin thickness seems to be controlled by the temperature for the highest thermal levels and by the stress level for the opposite case [17,18]. The values of Sa are basically determined by T_{inj} and Q_{inj} [18,28]. T_w has only a marginal effect, as can be seen in Table 2 (e.g. comparing the reference mouldings 200/5/40 to 200/80/40 and 270/5/5 to 270/80/5).

6.2.2. Skin morphology

In Fig. 5 the evolution of the morphological parameters of the skin (obtained by WAXS) with both thermal and mechanical levels is presented. The Debye-patterns reflect the bi-modal orientation of the shish–kebab structures. A significant variation of this structure with the thermomechanical environment is observed.

6.2.2.1. Level of orientation of the skin.

As observed in Fig. 5, the level of crystalline phase orientation of the skin, Ω_s, is higher for the higher values of τ_w, as reflected by the Debye patterns. The variations of Ω_s with the thermal and shear stress levels are shown in Fig. 6.

Ω_s increases markedly with the shear level, and it slightly decreases for high Y_c values. Ω_s is maximised for the thermomechanical environment leading to the highest τ_w and lowest Y_c. The variations are more accentuated for the

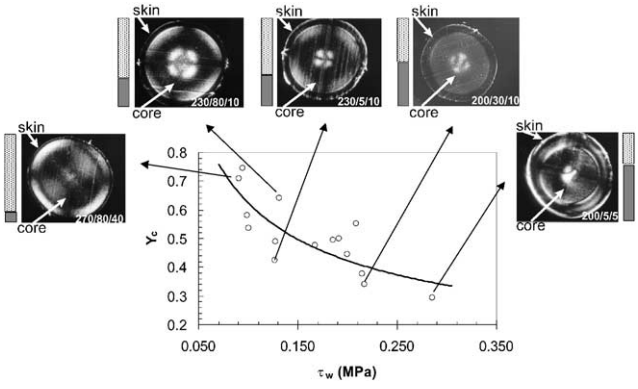

Fig. 3. Evolution of the skin ratio, Sa, with the thermal and shear stress levels (the bars compare relatively the correspondent values of Sa).

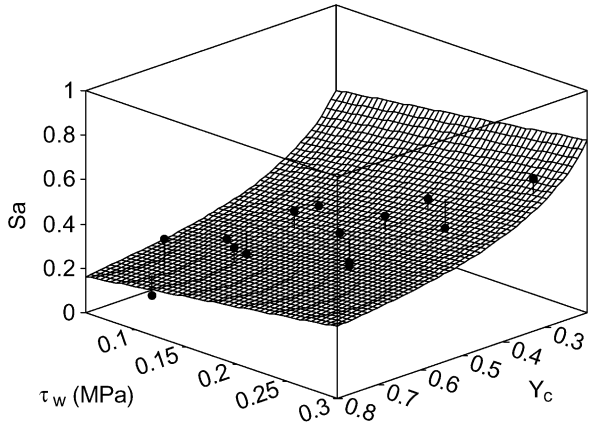

Fig. 4. Variation of the skin ratio, Sa, with the thermal and stress levels, Y_c and τ_w, respectively ($R^2 = 0.62$; R^2 is the coefficient of multiple regression).

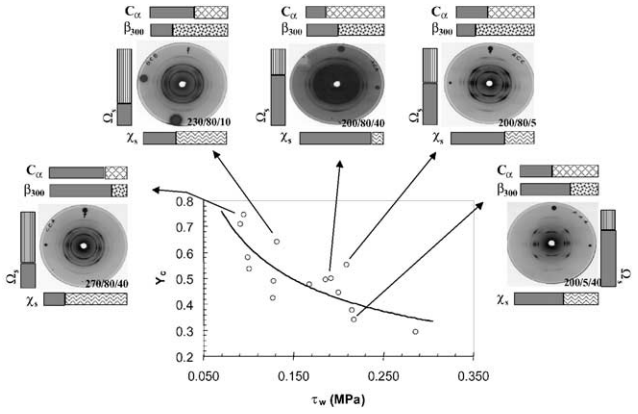

Fig. 5. Evolution of the morphological parameters of skin with the thermal and shear stress levels. The bars compare the relative values of the respective morphological parameter of the skin: Ω_s—crystalline phase orientation index, χ_s—degree of crystallinity, β_{300}—β-form index, C_α—double texture index. For selected mouldings are shown the respective WAXS diffracted pattern.

lowest shear stresses, tending for a plateau value for the highest τ_w.

Globally, the conditions with lower T_{inj} show the highest Ω_s. This processing variable has the strongest effect on the variations of Ω_s (e.g. comparing the processing conditions 200/30/10 and 270/30/10 in Table 2).

6.2.2.2. Degree of crystallinity of the skin.

In Fig. 7 are presented the variations of degree of crystallinity of the skin layer, χ_s.

The trends reflect the effect of shearing on the crystallization kinetics. In fact, χ_s increases both with Y_c and τ_w. Shearing was found to strongly increase the nucleation density and the growth rate during crystallization [37].

6.2.2.3. Double texture index of the skin.

The bimodal orientation of the crystalline phase (assessed by C_α) is, on the whole, higher for the highest Y_c values (Fig. 5). A higher C_α reflects a stronger orientation of the a^*-axis component relatively to the c-axis. Fig. 8 presents the variations of C_α with Y_c and τ_w.

The shear level basically determines the values of C_α. They decrease with τ_w, principally for the lowest shear stress levels. This means that the shear level increases the c-axis orientation component relatively to the a^*-axis component. However, for the highest τ_w values (beyond $\tau_w \approx 120$ kPa in Fig. 8), C_α is independent of τ_w, reaching a low plateau value ($C_\alpha \approx 0.42$). The $a*$-axis orientation component was found to increase with the melt temperature [10].

6.2.2.4. β_{300}-form contents.

The amount of β-phase in the skin is very small (index β_{300}), but nevertheless, dependent on the processing conditions. The skin crystallises essentially in the α-form, although a small amount of β-form can also be found. Nevertheless, it seems interesting to analyse the variations of the β_{300} index with processing. β_{300} index is higher for

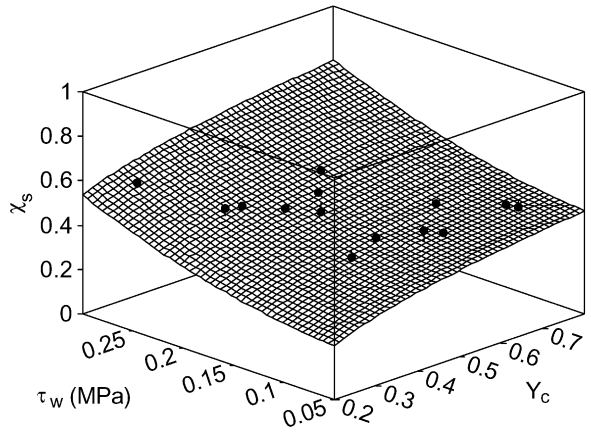

Fig. 7. Variation of the skin degree of crystallinity, χ_s, with the thermal and stress levels, Y_c and τ_w, respectively ($R^2 = 0.74$; R^2 is the coefficient of multiple regression).

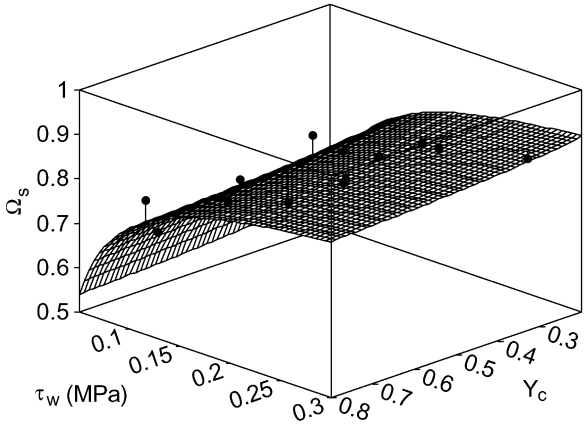

Fig. 6. Variation of the skin orientation level, Ω_s, with the thermal and stress levels, Y_c and τ_w, respectively ($R^2 = 0.72$; R^2 is the coefficient of multiple regression).

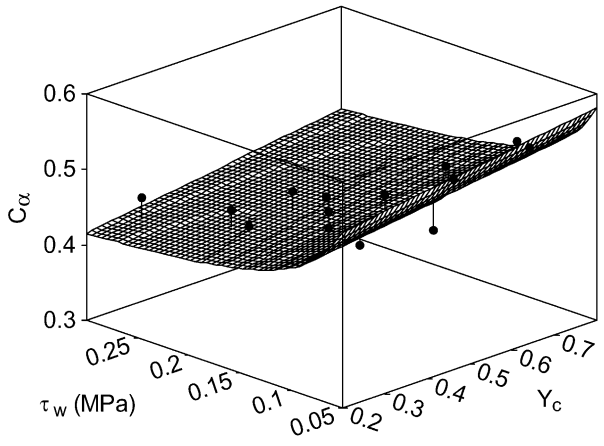

Fig. 8. Variation of the double texture index of the skin, C_α, with the thermal and stress levels, Y_c and τ_w, respectively ($R^2 = 0.54$; R^2 is the coefficient of multiple regression).

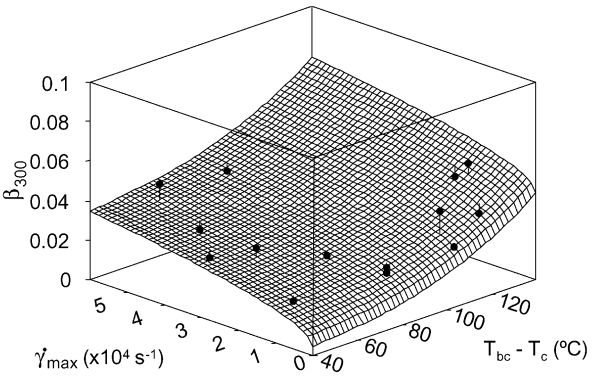

Fig. 9. Variation of β-form content index of the skin, β_{300}, with the temperature difference ($T_{bc} - T_c$), and the maximum shear rate, $\dot{\gamma}_{max}$ ($R^2 = 0.79$; R^2 is the coefficient of multiple regression).

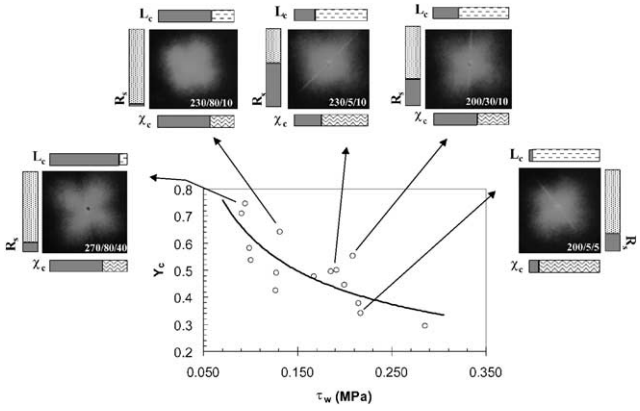

Fig. 10. Evolution of the morphological parameters of the core with the thermal and shear stress levels. The bars compare the relative values of the morphological parameters of the core layer: χ_c—degree of crystallinity, l_c—lamella thickness, and R_s—spherulite size. For selected mouldings are shown the respective SALS four-lobed pattern.

both the extreme limits of the thermomechanical environment (Fig. 5). The variations of this index with the thermal and shear stress levels are not very clear, the relationships presenting a very low coefficient of multiple correlation. In fact, it seems that the amount of β_{300}-form is more dependent on the temperature difference $T_{bc} - T_c$ and on the shear rate rather than on Y_c and τ_w [28]. This is shown in Fig. 9, where β_{300} increases with both ($T_{bc} - T_c$) and $\dot{\gamma}_{max}$. The variations are higher with the thermal level. The melt temperature and the flow rate were found to be the main processing variables affecting β_{300} [10,38]. The amount of β-phase was observed to increase with the injection rate [8], for high temperatures gradients and large degree of superheating of the melt [39].

6.3. Core layer

Fig. 10 depicts the evolution of the core morphology with the thermal and stress levels. In general, χ_c and l_c both decrease with the decrement of Y_c. The four-lobed scattering patterns are not well defined, which can be attributed to the heterogeneous morphology developed under processing (distribution of spherulite sizes, impingement and incomplete growth of the spherulites and their internal disorder) [29] and/or to multi-scattering phenomena (high thickness of the microtomed samples, 15 μm, compared to the estimated size of the scattering objects, 2–3 μm). This leads to the experimental difficulty on the localization of the maximum intensity locus. Anyway, the average spherulite size, R_s, is inversely proportional to the size of the scattered pattern. The variations of R_s present a complex dependence on the thermomechanical environment (Fig. 10).

The general trend is an unexpected reduction of R_s with Y_c. Nevertheless, a better definition of the four-lobed pattern is observed for the highest Y_c, revealing the possible development a more perfect and homogeneous spherulitic structure.

6.3.1. Degree of crystallinity of the core

The core crystallises in quasi-static conditions. So, the crystallization kinetics would be determined mainly by the thermal level, Y_c (although the previous shearing history influences the crystallisation kinetics [37]). Fig. 11 shows the variation of χ_c with the temperatures differences contributing for Y_c.

A higher χ_c is obtained for the lowest values of ($T_{bc} - T_i$) and highest ($T_{bc} - T_c$). However, it seems that the former temperature difference ($T_{bc} - T_i$ is proportional to the cooling rate) has the strongest effect. It has been observed that the degree of crystallinity is basically governed by the cooling rate and the melt temperature [11]: it decreases with increasing cooling rate and for low melt temperatures.

6.3.2. Thickness of the core lamella

Fig. 12 presents the variations of the thickness of the core lamella, l_c, with both temperatures differences. Thicker lamellas are obtained for the lowest ($T_{bc} - T_i$) and highest ($T_{bc} - T_c$), these conditions also leads to higher core crystallinity. However, the thickness of lamellas is more dependent

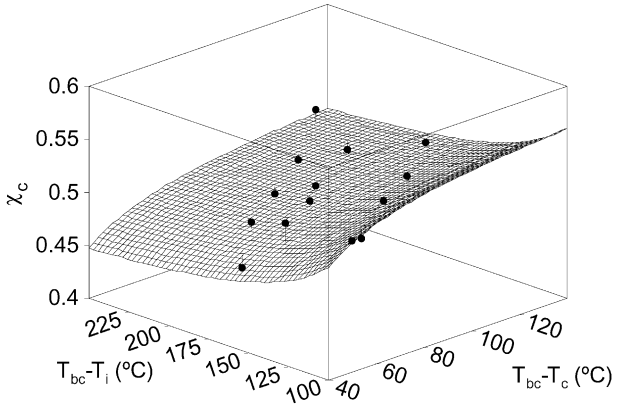

Fig. 11. Variation of the core degree of crystallinity, χ_c, with the temperature differences ($R^2 = 0.73$; R^2 is the coefficient of multiple regression).

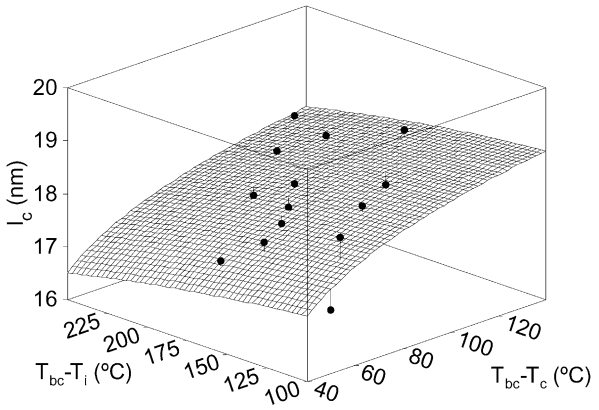

Fig. 12. Variation of the thickness of the core lamella, l_c, with the temperature differences ($R^2 = 0.69$; R^2 is the coefficient of multiple regression).

upon $(T_{bc} - T_c)$. In fact, the undercooling degree is the major factor determining the values of l_c [25].

7. Discussion

7.1. Skin thickness

The skin is the result of crystallisation under high stress fields and cooling rates. The molecular orientation induced by the flow cannot completely relax before the temperature reaches T_c, constraining the development of the crystalline structure. In this case, highly oriented structures are formed (shish–kebab structure); otherwise spherulites are developed. Demiray et al. stated that the skin thickness is controlled by the material relaxation time and the cooling rate [11]. A minimum shear level is also associated with the skin formation [17,40]. The skin development can then be related to two factors:

(i) the time allowed for relaxation until T_c is reached, t_r;
(ii) the relaxation time of the material, λ.

If the crystallisation temperature is reached before all the molecular relaxation takes place, then a highly oriented structure is formed (skin layer). Generalising, it can be assumed that:

1. if $t_r > \lambda$, then the flow induced orientation is able to completely relax and a spherulitic structure is developed;
2. if $t_r < \lambda$, then the flow induced orientation has not enough time to relax before crystallisation, leading to the formation of the skin (highly oriented structure).

Skin thickening is then promoted by lower t_r and higher λ values. The opposed conditions leads to skin thinning. Fig. 13 resumes the main factors contributing for the development of the skin. It is always assumed the formation of a skin layer, that is $t_r < \lambda$.

The thermal level (proportional to Y_c) determines the values of t_r and λ (the variables controlling the skin development). A high Y_c results in higher t_r. This can be accomplished by a higher $(T_{bc} - T_c)$ or a reduced $(T_{bc} - T_i)$ temperature differences. In the definition of Y_c, the crystallisation temperature was assumed constant. However, it depends on the cooling rate, decreasing with it. It is considered that the relative reduction of T_c for lower cooling rates (with consequent marginal increasing of Y_c due to the increment of $(T_{bc} - T_c)$) is of secondary importance, comparing with the effect of $(T_{bc} - T_i)$ itself. The thermal level also determines λ, which decreases with increasing temperature. Therefore, to a higher thermal level corresponds always a thinner skin.

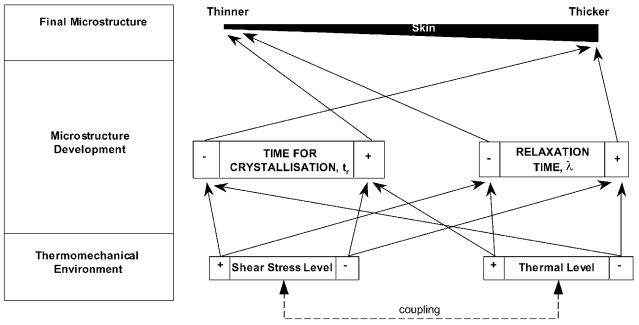

Fig. 13. Factors affecting the development of the skin thickness.

The shear stress level governs mainly the crystallisation temperature and the relaxation time of the material. Shearing was found to increase the T_c remarkably. This increase causes a reduction on t_r, with a consequent thicker skin. But, a higher shearing reduces also the value of λ, enhancing the tendency for skin thinning. The influence of the shear stress level on the skin development is complex, being determined by the balance between these two opposed effects.

In injection moulding the thermal and shear stress levels are strongly coupled. The degree of this coupling also determines the relative importance of these levels on the skin development.

The proposed mechanisms (Fig. 13) explain the evolution of Sa observed in Fig. 4. To a higher thermal level (Y_c) corresponds always a thinner skin due to the lower λ and higher t_r. The shear stress level is expected to determine in more extension the increase on T_c, rather than the reduction of λ. Furthermore, the thermal and stress levels are strongly coupled (Fig. 1): to a high shear stress level corresponds a lower thermal level. This will result in a thicker skin layer for the highest τ_w.

7.2. Skin morphology

The final orientation level of the skin is the result of what can be oriented during flow (related to the stress level) to what can relax until T_c is reached (time for relaxation). A high molecular orientation imposed during the filling phase will be automatically frozen in if the time for relaxation is significantly reduced (e.g. high cooling rate). Fig. 14 shows

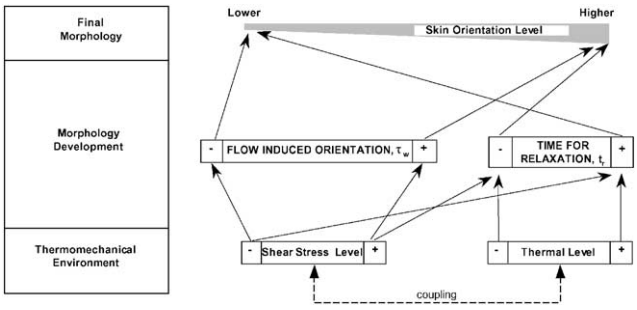

Fig. 14. Factors affecting the development of the level of orientation of the skin.

the main mechanisms contributing for the development of the level of orientation of the skin (it is assumed that $t_r < \lambda$).

A high thermal level (Y_c) leads to a higher time for relaxation, as has been described above, and therefore in a lower final orientation. High shearing will result in a higher molecular orientation induced by flow. It also leads to a decrement on t_r, due to the increase on T_c, as seen above. This results in a final higher level of orientation. The variations of Ω_s with the thermal and the shear stress levels in Fig. 6 are in agreement with the mechanisms described. The final level of orientation is then the balance between what can be oriented to what the can be relaxed. The definition of a thermo-stress index, τ_{Ys}, aimed at relating these two quantities [18,28,36,41,42]:

$$\tau_{Y_s} = \frac{\tau_w}{Y_s} \tag{6}$$

where Y_s is defined analogously as Y_c (Eq. (5)), but considering the average temperature of the skin, T_{bs}. The variations Ω_s with τ_Y are presented in Fig. 15. In general trend, to a high τ_Y corresponds higher Ω_s values.

Comparing both Figs. 13 and 14, a thicker skin is, in general, more oriented, but this must not be considered as the general case. In fact, situations may exist that will result in a thinner and simultaneously more oriented skin. For example, a higher stress level may lead to a more oriented skin but at the same time thinner due to the reduction on the material relaxation time (for equivalent thermal levels).

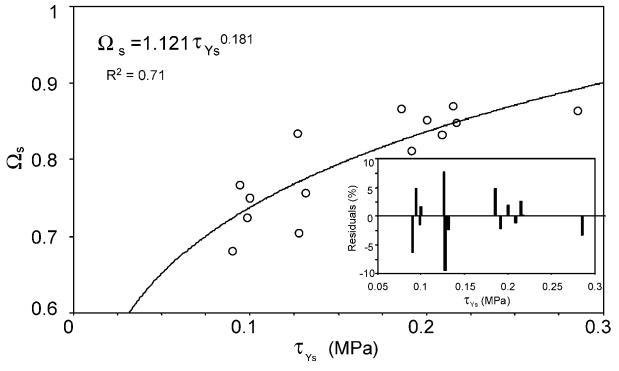

Fig. 15. Evolution of the skin crystalline phase orientation index, Ω_s, with the thermo-stress index τ_{Y_s} (the solid line is the fit obtained with the presented equation; R^2 is the coefficient of correlation; on the bottom right side is shown the correspondent residuals graph).

7.3. Core morphology

The crystallisation is a phase transformation occurring in two stages: nucleation and the subsequent growth of the crystalline structures within the untransformed volume. The core can be assumed to crystallise in almost quiescent conditions. Therefore, the influence of the shear stress level can be disregarded (although shearing affects the crystallisation kinetics even after the cessation of the flow [37]).

The slower crystallisation process of the core is mainly thermally controlled. The final degree of crystallisation is the result of the competition between growth rate and the cooling rate (affecting the nucleation). According to Fig. 11, χ_c increases with ($T_{bc} - T_c$), which is expected to lead to a higher growth and lower nucleation rates (respectively, $\dot{G}$ and $\dot{N}$). On the other hand, χ_c decreases with ($T_{bc} - T_i$), due to the expected strong increase on $\dot{N}$. In fact, this seems to be the factor with the strongest effect. The variations of l_c with both temperature differences (Fig. 12) are similar to that of χ_c. However, the influence of ($T_{bc} - T_c$) is more accentuated. Here the governing factor seems to be the degree of undercooling.

A relationship between R_s and the thermomechanical variables is rather difficult to establish due to the large errors on the experimental measurements. Nevertheless, some unexpected results were already anticipated (see Fig. 10), R_s decreasing with Y_c. This even result may be mainly attributed to:

- A longer application of the holding pressure (larger gate sealing time) due to a higher Y_c; the effect of the pressure is to shift the crystallisation kinetics to the higher temperatures [43]; a reduction of the spherulite diameter with increasing pressure was reported for bulk samples [44], due to an increase on the thermodynamic melting temperature and consequently on the undercooling degree.
- An increase of the nucleation rate with Y_c; the change on the nucleation rate with the temperature has a convex shape; at higher undercooling degrees the process is diffusion controlled (left side of the curve), where an increase on the temperature (lower undercooling) results in a higher nucleation rate, and thus on spherulites of smaller dimensions.

Anyway, R_s is an average value of the distribution of spherulites sizes. The unexpected variations may indicate that the assessment of spherulite size of the core should not be performed in bulk samples. Cutting through-the-thickness slices along the core and taking the respective scattered patterns should accomplish a more exhaustive analysis.

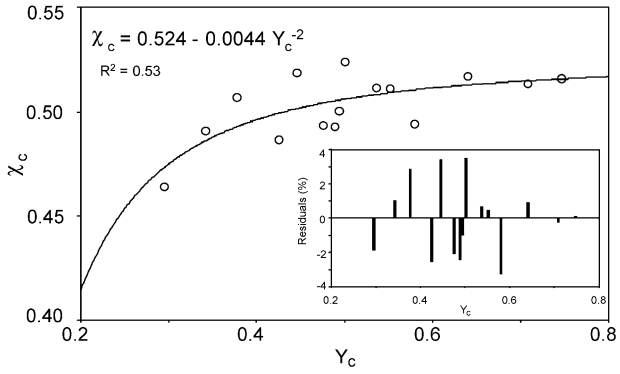

Fig. 16. Trend of evolution of the core degree of crystallinity, χ_c, with the cooling index Y_c (the solid line is the fit obtained with the presented equation; R^2 is the coefficient of correlation; on the bottom right side is shown the correspondent residuals graph).

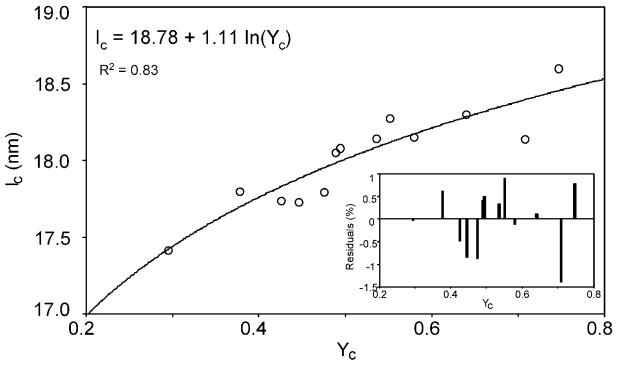

Fig. 17. Variation of thickness of core lamella, l_c, with the cooling index Y_c (the solid line is the fit obtained with the presented equation; R^2 is the coefficient of correlation).

The cooling index, Y_c, is the ratio between two temperatures differences (Eq. (5)). Its definition aimed at quantifying the crystalline morphology of the core [18,28,36,41,42]. The variations of χ_c and l_c with Y_c are shown in Figs. 16 and 17, respectively.

Both χ_c and l_c increase with Y_c, as already anticipated. The low coefficient of correlation of the χ_c model may be attributed to the inaccuracy of the experimental measurements. In fact, it was already demonstrated for another moulding and material (polyethylene) the close relationship between χ_c (determine by density measurements in this case) and Y_c [36].

In the definition of Y_c, T_c was assumed as constant. However, it depends on shearing, the cooling rate and pressure. It is expected that the further consideration of these effects and the accounting of the packing stage will lead to an improvement on the obtained correlations.

The two thermomechanical indices were already proposed as a valuable tool in establishment of relationships between the processing and the mechanical properties, as need in an industrial context [28,41]. Furthermore, the effect of processing was introduced on the coefficients of a constitutive equation through the use of the thermomechanical indices [28,42], allowing the prediction of the mechanical behaviour under different temperatures, strain rates and modes of loading.

8. Conclusions

For this moulding, the thermal and shear stress levels are strongly coupled: the former increases as the latter decreases. The effect of the thermomechanical environment on the development of the microstructural features of the skin and core is resumed in Table 3.

For the mouldings and processing window used, the following relationships were established:

- The skin ratio, Sa, increases with the stress level, τ_w and decreases with the thermal one, Y_c.
- The level of orientation of the skin, Ω_s, increases with τ_w and decreases with Y_c. The influence of the former is more accentuated.
- The degree of crystallinity of the skin, χ_s, increases with both Y_c and τ_w.
- The double texture index of the skin, C_α, is mainly dependent on τ_w, decreasing with it, mainly for low τ_w values. Shearing increases the *c*-axis orientation component

Table 3
Effect of the variation of the thermomechanical conditions on the development of the microstructure (the double arrows mean a stronger effect) (Var.—sense of variation, Y_c—cooling index, T_{bc}—bulk temperature, T_c—crystallization temperature, T_w—mould temperature, τ_w—wall shear stress, τ_{Y_s}—thermo-stress index, $\dot{\gamma}_{max}$—maximum shear rate, Sa—skin ratio, Ω_s—skin orientation index, χ_s—degree of crystallinity of the skin, C_α—double texture index of the skin, β_{300}—β-phase index of the skin, χ_c—degree of crystallinity of the core, l_c—lamella thickness of the core)

Thermomechanical environment		Var.	Skin					Core	
			Sa	Ω_s	χ_s	C_α	β_{300}	χ_c	l_c
Thermal level	$(T_{bc} - T_i)$	↗	–	–	–	–	▲▲	▲	▲▲
(Cooling index)	$(T_{bc} - T_w)$	↗	–	–	–	–	–	▲▲	▲
	Y_c	↗	▼	▼	▲	≈	–	▲	▲
Shear stress level, τ_w		↗	▲	▲▲	▲	▼▼	–	–	–
Shear rate, $\dot{\gamma}_{max}$		↗	–	–	–	–	▲	–	–
Thermo stress index, τ_{Y_s}		↗	–	▲	–	–	–	–	–

relatively of the a^*-orientation component up to a minimal limit. Thereafter C_α remains constant.

- The amount of β-form of the skin (evaluated by the β_{300} index), is mainly dependent on T_{bc} and the maximum shear rate, increasing with both. The variations are more pronounced with the former.
- The degree of crystallinity, χ_c, and the lamella thickness of the core, l_c, increase with the both temperature differences. The former is more dependent on $T_{bc} - T_i$ (cooling rate), whereas the latter on $T_{bc} - T_c$ (superheating degree).
- In general a thicker skin is simultaneously more oriented and crystalline. At the same time, the core is less crystalline with thin lamellae. This is the reflex of the strong thermomechanical coupling.

Furthermore, the development of the skin layer has been interpreted in the light of two main factors:

(i) the time allowed for relaxation until the crystallisation temperature is reached, t_r;
(ii) the relaxation time of the material, λ.

If $t_r < \lambda$, then a highly oriented crystalline structure is developed. The final level of molecular orientation of this structure (skin) is the result of what can be oriented during flow (related to the stress level) to what can relax until T_c is reached (time for relaxation). This ratio is related on the definition of the thermostress index, τ_{Y_s}, which estimates the level of orientation of the skin, Ω_s.

The final degree of crystallisation of the core is related to the competition between the grow rate and the cooling rate. The cooling index evaluates the crystallisation process of the core, reflecting the variations of χ_c and l_c.

The thermomechanical indices have been evidenced as a valuable tool in interpreting the development of the microstructure in injection moulding, justifying their use on the establishment of straightforward relationships between them and the mechanical properties of the mouldings.

References

[1] Kantz MR, Newman HD, Stigale FH. J Appl Polym Sci 1972;16:1249.
[2] Fitchmun DR, Mencik Z. J Polym Sci 1973;11:951.
[3] Katti SS, Schultz JM. Polym Engng Sci 1982;22(16):1001–17.
[4] Schultz JM. Polym Engng Sci 1984;24:770.
[5] Trotignon JP, Verdu J. J Appl Polym Sci 1987;34(1):1–8.
[6] Kamal MS, Moy FH. Polym Engng Rev 1989;2:381.
[7] Fujiyama M, Wakino T. Int Polym Proc 1992;VII(1):97–105.
[8] Cunha AM, Pouzada AS, Crawford RJ. Plast Rubber Comp Proc Appl 1992;18(2):79–90.
[9] Phillips R, Herbert G, News J, Wolkowicz J. Polym Engng Sci 1994;34(23):1731–43.
[10] Fujiyama M. In: Karger-Koscis J, editor. Polypropylene structure, blends and composites: structure and morphology, vol. 1. London: Chapman & Hall, 1995. p. 167–204.
[11] Demiray M, Isayev AI. SPE ANTEC Technical Papers. ANTEC'96; 1996.
[12] Zipper P, Abuja PM, Jánosi A, Wrentschur E, Geymayer W, Ingolic E, Friesenbichler W. Polym Engng Sci 1996;36(4):467–82.
[13] Ayrom-Keuchel H, Cakmak M. SPE ANTEC Technical Papers. ANTEC'99, vol. II; 1999: 1910–5.
[14] Kalay G, Bevis MJ. J Polym Sci: Part B: Polym Phys 1997;35:265–91.
[15] Fujiyama M, Wakino T, Kawasaki Y. J Appl Polym Sci 1988;35:29–49.
[16] Wening W, Herzog F. J Appl Polym Sci 1993;50:2163–71.
[17] Brito AM, Cunha AM, Pouzada AS, Crawford RJ. Int Polym Proc 1991;VI(4):370–7.
[18] Viana JC, Cunha AM, Billon N. Int Polym 1997;43:159–66.
[19] Zipper P, et al. Int Polym Proc 1995;X(4):341–50.
[20] Cunha AM, Pouzada AS. Impact and dynamic fracture of polymers and composites. In: Williams JG, Pavan A, editors. ESIS19London: Mech. Eng. Public, 1995. p. 315–25.
[21] Trotignon JP, Verdu J. J Appl Polym Sci 1990;39:1215–7.
[22] Burke M, Young RJ, Stanford JL. Plast Rubber Comp Proc Appl 1993;20(3):121–35.
[23] Sanschagrin B, Amdouini N, Fisa B. SPE ANTEC Technical Papers. ANTEC'91; 1991.
[24] Khanna YP. Macromolecules 1993;26:3639–43.
[25] Raults J. J Mater Sci, Rev Macromol Chem Phys 1997;C37(2):335–87.
[26] Saiu M, Brucato V, Piccarolo S, Titomanlio G. Int Polym Proc 1992;VII(3):267–73.
[27] CMOLD® Reference Manual, AC Technology; 1996.
[28] Viana JC. PhD thesis, University of Minho; 2000.
[29] Haudin J-M. In: Meeten GH, editor. Optical properties of polymers. London: Elsevier, 1989. p. 167–264.
[30] Monasse B, Haudin J-M. Colloid Polym Sci 1985;263:822–31.
[31] Mandelkern L, Alamo RG. In: Mark JE, editor. Physical properties of polymers handbook. New York: American Institute of Physics, 1996.
[32] Zhou H, Wilkes GL. Polymer 1997;38(23):5735–47.
[33] Dahoun A, Aboulfaraj M, G'Sell C, Molinari A, Canova GR. Polym Engng Sci 1995;34(4):317–29.
[34] Butler M, Donald AM, Ryan AJ. Polymer 1997;38(22):5521–38.
[35] Trotignon JP, Lebrun JL, Verdu J. Plast Rubber Proc Appl 1982;2(3):247–51.
[36] Cunha AM, Godinho JS, Viana JC. Structure development during polymer processing. In: Cunha AM, Fakirov S, editors. Nato Science Series, Series E: Applied Science, vol. 370. Dordrecht: Kluwer Academic Publishers, 2000. p. 255–77.
[37] Tribout C, Monasse B, Haudin J-M. Colloid Polym Sci. 1996;274:197–208.
[38] Zipper P, Jánosi A, Wrentschur E, Geymayer W, Ingolic E, Friesenbichler W, Eig F. Int Polym Proc 1997;XII(2):192–9.
[39] Phillips RA, Wolkowicz MD. In: Moore EP, editor. Polypropylene handbook, Munich: Hanser, 1996. p. 113–76.
[40] Isayev AI, Xiaoping G, Luo G, Demiray M. SPE ANTEC Technical Papers, ANTEC'97, USA; 1997
[41] Viana JC, Cunha AM. SPE ANTEC Technical papers, ANTEC'2000, USA; 2000.
[42] Viana JC, Cunha AM, Billon N. Polym Engng Sci 1999;39(8):1463–72.
[43] Phillips PJ, Campbell RA. SPE ANTEC Technical Papers, ANTEC'91; 1991. p. 896–9.
[44] Reinshangen JH, Dunlap RW. J Appl Polym Sci 1973;17:3619–25.